



ORIGINAL ARTICLE

Surface behavior and photocatalytic property of $\text{Co}_{1-x}\text{Zn}_x\text{Fe}_2\text{O}_4$ nanoparticles synthesized by a hydrothermal method

H.-Y.He

College of Materials Science and Engineering, Shaanxi University of Science and Technology, Xi'an, Shaanxi, 710021, (CHINA)

E-mail: hehy@sust.edu.cn

Received: 30th June, 2013 ; Accepted: 22nd August, 2013

Abstract : The cobalt zinc ferrite $\text{Co}_{1-x}\text{Zn}_x\text{Fe}_2\text{O}_4$ ($x=0-1.0$) nanoparticles were synthesized by a hydrothermal method. Effects of zinc content on the microstructure, surface alkaline-acidic behavior and photocatalytic property of the nanoparticles were studied. The oxidation-reduction potential of methyl blue aqueous solution in presence of the nanoparticles at pH=7 under natural sunlight irradiation is obviously negative and increased with increase in Zn content. The degradation rate of methyl blue in aqueous solution on the

nanoparticles also decreases as increase in Zn content in sunlight. The variations of the oxidation-reduction potential and photocatalytic efficiency with Zn content were discussed on basis of the light absorbance, microstructure, and physicochemical characteristics of the nanoparticles.

Keywords : Nanostructured materials; Optical spectroscopy; Oxidation reduction potential; Photocatalytic property.

INTRODUCTION

Spinel ferrite nanoparticles have narrow band gap energy (~2.0 eV), so their nanoparticles are potential photocatalysts for the decontamination of environment because of their superiority in full utilization of nature light. Many studies have showed that some ferrite nanoparticles exhibited excellent photocatalytic activity^[1,2]. Recent studies further indicated that composites of different ferrites^[2] and ferrite with other photocatalysts^[3,4] possess more efficiency than single one.

Excepting light absorption, initial pH of water environment and irradiation light resource et al can also affect the activity of the photocatalysts^[5]. Some studies have indicated that the oxidation-reduction characterizations of the photocatalyst surface and its evident variation caused by acidic-alkaline and light irradiation of environment have considerable influence on the activity of the catalysts and photocatalysts^[6-12].

To date, many methods have been developed to prepare spinel ferrite nanopowders, such as aerosol route^[13], the co-precipitation method^[14,15], the usual ceramic technique^[16], the hydrolysis method^[17], the mi-

crowave-hydrothermal method^[18], and the hydrothermal method^[19]. The hydrothermal method is widely used because of its simple process, low cost, low synthesis temperature, and small particle size, less thermal stress, and less internal defect of synthesized powders^[19].

In the current study, we focus on the hydrothermal synthesis of $\text{Co}_{1-x}\text{Zn}_x\text{Fe}_2\text{O}_4$ nanoparticles and examining the effect of the zinc content on microstructure, surface alkaline-acidic behavior, and photocatalytic property of the synthesized nanoparticles

EXPERIMENTAL

Cobalt chloride ($\text{CoCl}_2 \cdot 6\text{H}_2\text{O}$, Hebei Kingway Chemical Industry Co. Ltd. China), zinc nitrate ($\text{Zn}(\text{NO}_3)_2 \cdot 6\text{H}_2\text{O}$, Shenyang Hua Bai Tai Chemical Co. Ltd, China), and iron nitrate ($\text{Fe}(\text{NO}_3)_3 \cdot 9\text{H}_2\text{O}$, Beijing Baishunchem. Co. Ltd., China) were used as starting materials. The chemicals used were all analytical agent without further processing. The chemicals were weighed according to the required stoichiometric proportions of $\text{Co}_{1-x}\text{Zn}_x\text{Fe}_2\text{O}_4$ ($x=0, 0.2, 0.4, 0.6, 0.8, \text{ and } 1.0$) and dissolved in deionized water with same volume. The concentration of Fe^{3+} in the 20ml solution was 0.02 mol l^{-1} . NaOH with double gram equivalent of all metal cations was dissolved in small amount of deionized water and completely dropped into the solutions with magnetic stirring. This relative large amount of NaOH addition can assure the solution $\text{pH} > 10$ throughout and so full precipitation of all cations. The precursor solutions were then transferred into autoclaves (volume: 25 ml, degree of filling: 80 vol.%) and filled to 20 ml with deionized water. After sealing, the hydrothermal reaction was then carried out in hydrothermal ovens at $180 \text{ }^\circ\text{C}$ for 24 h. Heating rate was about $30 \text{ }^\circ\text{C} \cdot \text{min}^{-1}$. After natural cooling in furnace, the products were washed repeatedly with distilled water, and then dried at $100 \text{ }^\circ\text{C}$ for 24 h.

The crystalline structure and phase of the synthesized $\text{Co}_{1-x}\text{Zn}_x\text{Fe}_2\text{O}_4$ nanoparticles was identified at room temperature using X-Ray diffractometer (XRD, $\text{CuK}_{\alpha 1}$, $\lambda=0.15406 \text{ nm}$, Model No: D/Max—2200PC, Rigaku, Japan). The particle size of the nanoparticles was determined by software Jade 5 provided with the diffractometer. This determination is based on well known Scherrer's equation. The morphology of the nanoparticles was analyzed using scanning electron mi-

croscopy (SEM, Model No: JXM-6700F, Japan). Fourier transform infrared spectra of the nanoparticles were measured with fourier transform infrared spectrometer (FTIR, Model no: VERTEX 70, Bruke, German). KBr was used as matrix to disperse the ferrite powder for compressing disk sample.

In this study, methyl blue was used as a catalytic substrate to study photocatalysis of the nanoparticles. In each experiment, 100 ml methyl blue aqueous with a concentration of $1 \times 10^{-5} \text{ M}$ was added into a glass beaker containing 50 mg one of nanoparticle. The aqueous solution was then dispersed for 5 min with an ultrasonic generator (UG, 40kHz, Model No: KQ-5200DE, China) at 100 W. The photocatalysis experiment was carried out under irradiations of sunlight in may and at the initial $\text{pH}=7$ of the methyl blue aqueous solution. The intensity of sunlight when they reach surface of the solutions was determined with a solar power meter (Model no: SM206, China) and is $\sim 800 \text{ W/m}^2$. After leaving to steady state in dark for 30 min and afterward each irradiation time of 1 h, $\sim 5 \text{ ml}$ solution was took out and filtrated out the suspended tiny particles and subsequently measured for their diffuse-reflection absorbance on a spectrophotometer (Model No: WFZ-900D4, China). The solution after the test was returned to the breaker to maintain the normal volume of the solution under test. The variation in oxidation-reduction potential of the methyl orange aqueous solution due to presence of the nanoparticles in the sunlight was determined by measuring the oxidation-reduction potential values of the solution with and without containing the nanoparticles on an oxidation-reduction potential tester (ORP-286, China) and afterward calculating their differences.

RESULTS AND DISCUSSION

XRD analysis

Figure 1 shows the XRD patterns of the synthesized nanoparticles. All diffraction peaks are consistent with standard powder diffraction data of spinel ferrites including Fe_3O_4 (JCPDS: 79-1744), indicating that the nanoparticles were composed of single phase $\text{Co}_{1-x}\text{Zn}_x\text{Fe}_2\text{O}_4$ without any other impurities. Lattice parameter of the nanoparticles are calculated with XRD data

ORIGINAL ARTICLE

analysis and show in Figure 2. They overall slightly increase with increase in Zn content. The average particle sizes of the nanoparticles are also determined from XRD data analysis and are in range of 10.5-15.0 nm that overall decreases with increase in Zn content.

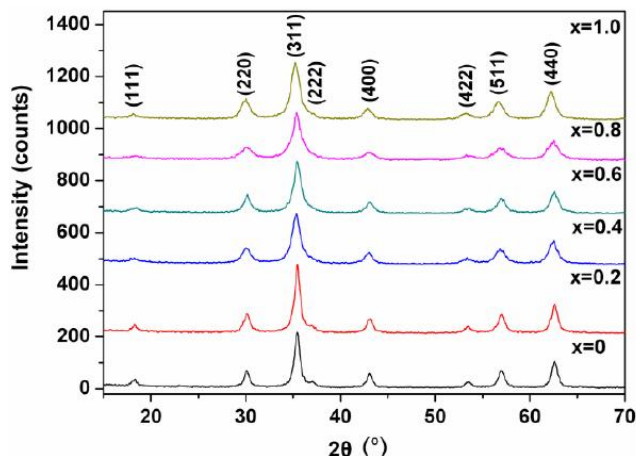


Figure 1 : XRD patterns of the $\text{Co}_{1-x}\text{Zn}_x\text{Fe}_2\text{O}_4$ nanoparticles

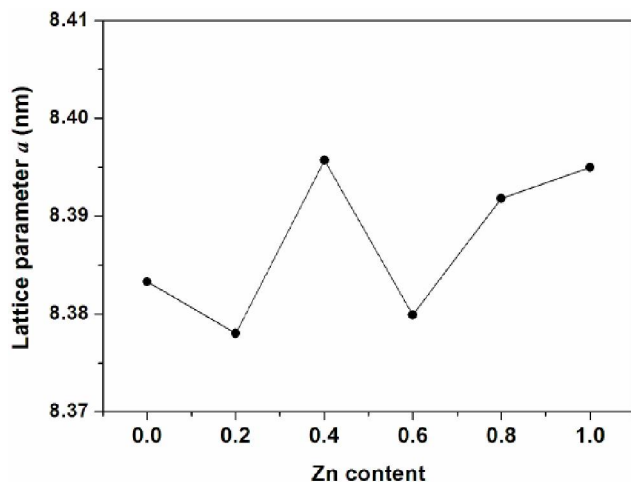


Figure 2 : Variation of lattice parameter of the nanoparticles determined with XRD analysis with Zn content

SEM analysis

The morphology of the $\text{Co}_{1-x}\text{Zn}_x\text{Fe}_2\text{O}_4$ nanoparticles was determined by SEM analysis. Figure 3 shows typical SEM micrographs of the nanoparticles. The particles of the nanoparticles are spherical with somewhat agglomerate. From the SEM micrographs of the nanoparticles, the average particle size is in a range of ~20.5-32.0 nm. They are illustrated in Figure 4 together with that analyzed from XRD data analysis. The estimated average particle sizes overall decreases with increase in Zn content (x). Figure 5 shows the SEM micrograph of a TiO_2 nanorods synthesized by a hy-

drothermal process. This nanorods shows a average particle size of ~15 nm and ~70 nm estimated from XRD and SEM, respectively. The sizes estimated from SEM micrographs are obviously larger than the result of XRD analysis, which could shows that these nanoparticles are polycrystalline.

FTIR analysis

Figure 6 shows the FTIR spectra of the nanoparticles. The broad peak observed at $\sim 3424\text{ cm}^{-1}$ is attributed to the stretching vibration of surface hydroxyls absorbed on surface and O-H groups in absorbed water, which indicates the adsorbed moisture^[20]. The peaks at $\sim 1622\text{ cm}^{-1}$ and $\sim 1359\text{ cm}^{-1}$ are assigned to H-O-H bending vibration in water molecular^[21] or OH deformation vibration due to surface hydroxyls^[22,23]. These imply good hydrophilicity that is favorable to the photocatalytic activity of the nanoparticles. The weak peak at 1092 cm^{-1} could be assigned to the C-O stretching^[24] due to adsorbed CO_2 . The two peaks at $\sim 576\text{ cm}^{-1}$ and below 400 cm^{-1} are assigned as the vibration of ferrite groups^[25], corresponding to the tetrahedral and octahedral sites of positive ions in the ferrite, respectively^[21,26]. The absorption peak centered at 576 nm overall shifts to low wavenumber as increase in Zn content. This can be ascribed to the increase in distance between $\text{Fe}^{3+}-\text{O}^{2-}$ in the tetrahedral sites. This confirms the formation of $\text{Co}_{1-x}\text{Zn}_x\text{Fe}_2\text{O}_4$ structure.

Optical absorption analysis

Figure 7 shows the diffuse-reflection absorbance spectra of the ferrite nanoparticles. The absorbance in UV-visible region increases with decrease in Zn content. The absorption edges of the ferrite nanoparticles are estimated to be ~710 nm, ~685 nm, 670 nm, 660 nm, 640 nm, and ~610 nm, corresponding to the band gap energies of ~1.75 eV, ~1.80 eV, ~1.85 eV, ~1.88 eV, ~1.94 eV, and ~2.03 eV, for Zn content of 0 at.%, 0.2 at.%, 0.4 at.%, 0.6 at.%, 0.8 at.%, and 1.0 at.%, respectively.

Oxidation-reduction potential of the nanoparticles surface

The acidic-alkaline behavior of a photocatalyst surface is usually evaluated by oxidation-reduction potential. Therefore, the variation in oxidation-reduction potential of the methyl blue aqueous solution with $\text{pH}=7$

due to the presence of the nano-particles (ORP) was measured under the sunlight. The measured results are show in Figure 8. The ORP of methyl blue aqueous solution in presence of the TiO_2 nanorodes similarly determined under same condition equals to -170 mV. The ORP are all larger negative value, implying a re-

ductive characterization of the nanoparticles surface in the photocatalytic experimental conditions. The reductive characterizations could come from stronger sunlight irradiation^[27,28]. Moreover, the ORP increases with increase in Zn content. This can be ascribed to higher Mulliken's electronegativity of Zn (4.70 eV) than Co

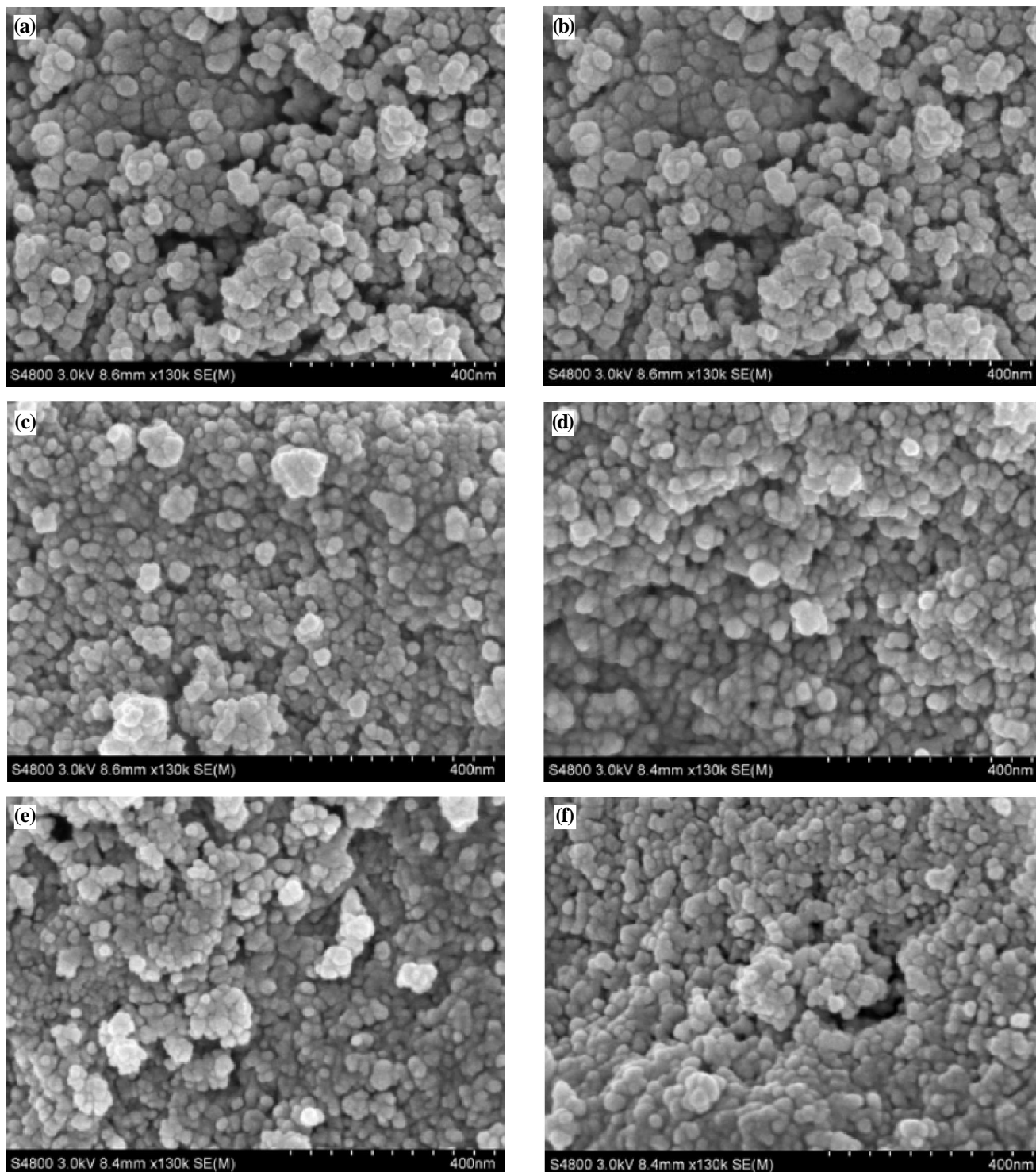


Figure 3 : SEM micrographs of the $\text{Co}_{1-x}\text{Zn}_x\text{Fe}_2\text{O}_4$ nanoparticles. $x=(a)0$, (b)0.2, (c)0.4, (d)0.6, (e)0.8, and (f)1.0

ORIGINAL ARTICLE

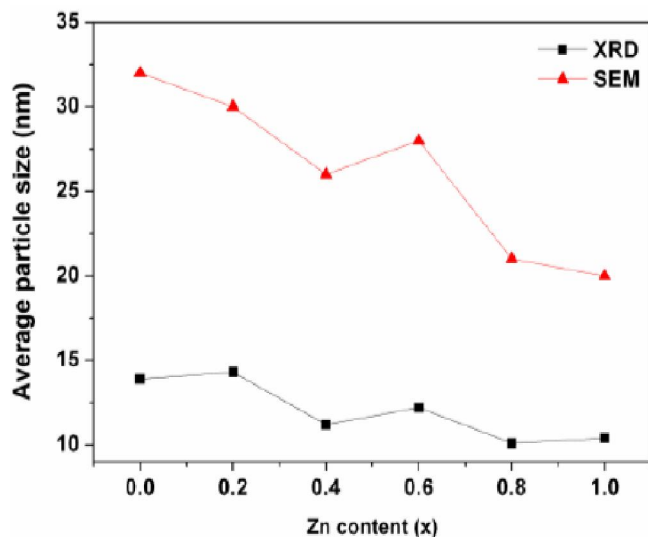


Figure 4 : Average particle size of the $\text{Co}_{1-x}\text{Zn}_x\text{Fe}_2\text{O}_4$ nanoparticles determined from XRD data analysis and SEM

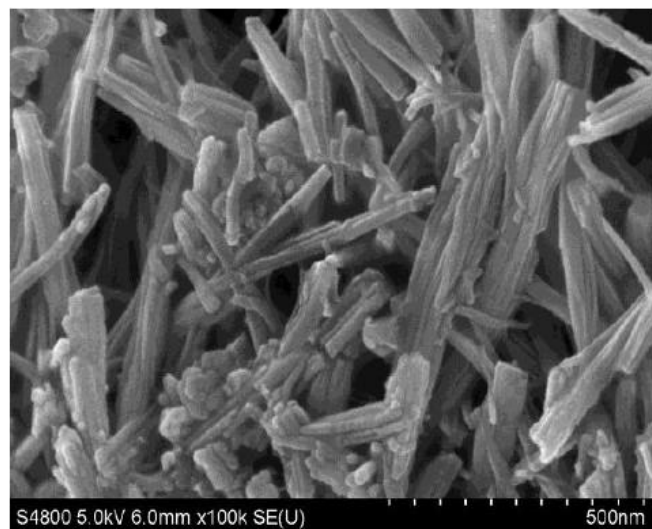
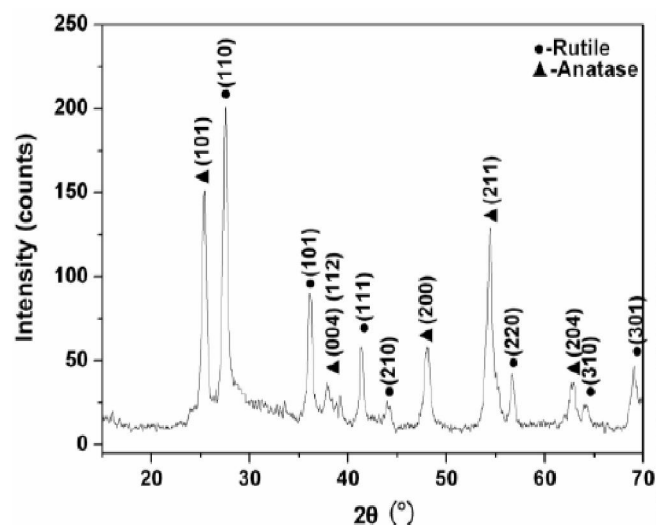


Figure 5 : XRD pattern and SEM micrograph of the TiO_2 nanorods.

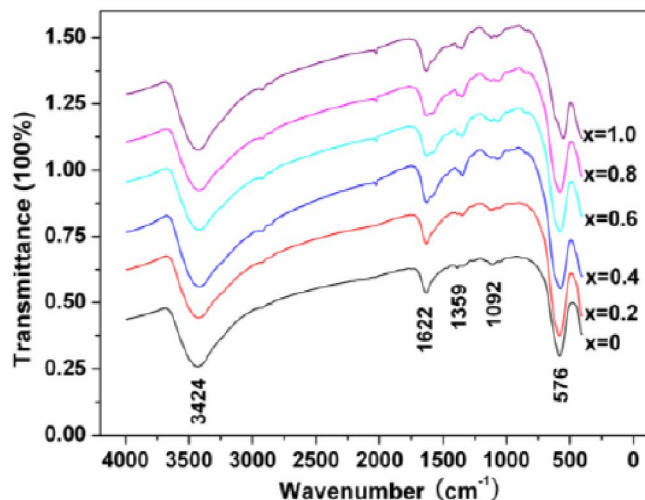


Figure 6 : FTIR spectra of the $\text{Co}_{1-x}\text{Zn}_x\text{Fe}_2\text{O}_4$ nanoparticles

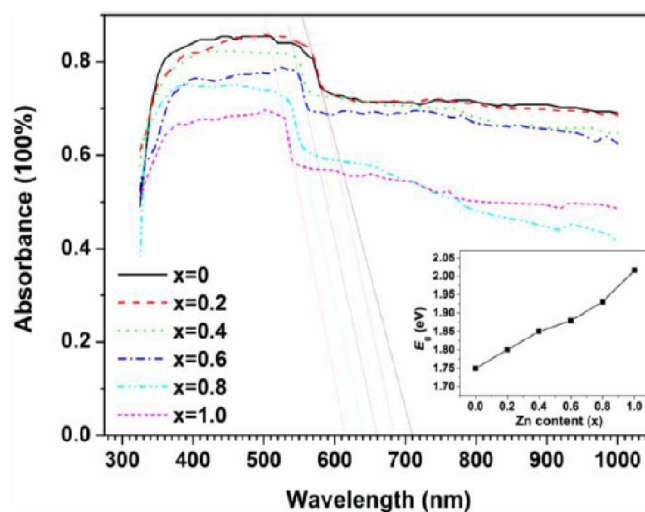


Figure 7 : Diffuse-reflection absorbance spectra of the $\text{Co}_{1-x}\text{Zn}_x\text{Fe}_2\text{O}_4$ nanoparticles. Inserted figure is the plot of band gap of the nanoparticles vs. Zn content

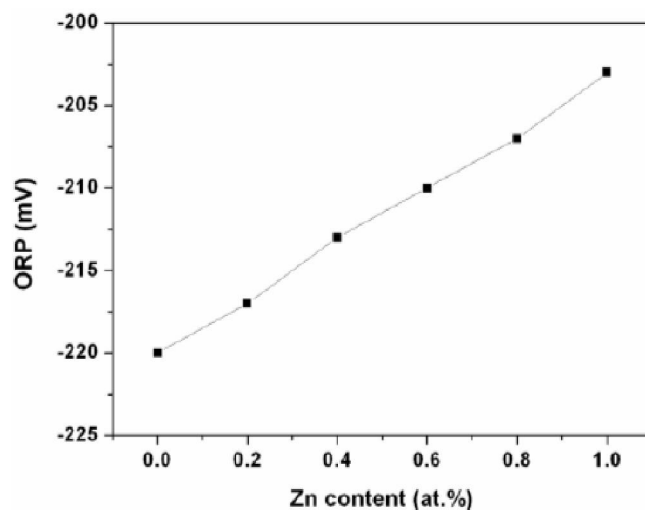


Figure 8 : ORP variation of methyl blue aqueous solution under sunlight irradiation with Zn content

(4.27 eV) and decreased light absorbance and increased lattice parameter with increase in Zn content^[10-12]. More explanation for the variation trend of the ORP is not found in previous literature and remains to be made.

Photocatalysis of the nanoparticles

Figure 9 shows the concentration variations of the methyl blue aqueous solutions on the ferrites nanoparticles with the irradiation times in the sunlight. The concentrations decrease with increase in times in different rates. The degradation rates decrease as increase in Zn content. This is agree to the increase in the ORP depended on the light absorbance and intrinsic behavior of the nanoparticles. A comparative study indicates that the photodegradation on the TiO₂ nanorods is slower than on the nano-ferrites, agreeing to its higher ORP. In addition, a contrast experiemnt indicates that the degradation efficiency of methyl orange in water on the ferrite nanoparticles is obvuious smaller than that of methyl blue in water. This may be due to less acidic sites of methyl orange (C₁₄H₁₄N₃NaO₃S) than the methyl blue (C₃₇H₂₇N₃Na₂O₉S₃).

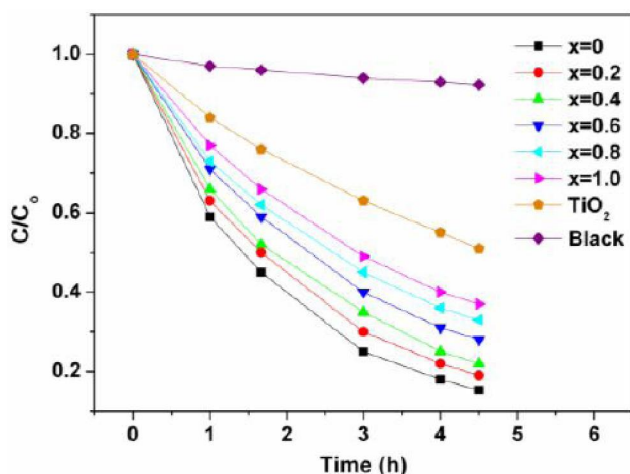


Figure 9 : Concentration variation of methyl blue aqueous solution on the Co_{1-x}Zn_xFe₂O₄ nanoparticles with irradiation time of sunlight (~800 W/m²)

In general, kinetic relation between the concentration (C) of the methyl blue solution and the photocatalytic reaction time (t) can be given by:

$$\frac{C}{C_0} = A \exp\left(-\frac{kt}{T}\right)$$

In which, C₀ is initial concentration, k is quasi-kinetic rate constant, T is reaction temperature and A is a constant. Figure 10 shows an approximately linear plots of

$-\ln(C/C_0)$ versus t for all the experiments. The values of k can be obtained directly from the linear regression analysis of the plots. The calculated k values for the photodegradation on the the ferrite nanoparticles decrease from ~1.92 h⁻¹ to ~1.03 h⁻¹ as increase in Zn content and are ~0.67 h⁻¹ for the TiO₂ nanorods.

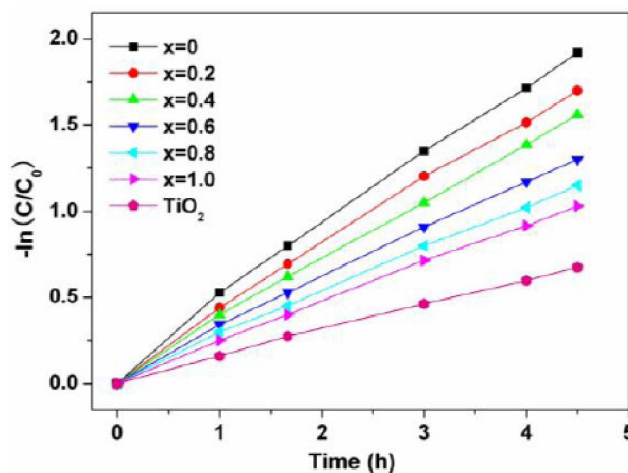


Figure 10 : The plots of $-\ln(C/C_0)$ vs. irradiation time of sunlight

CONCLUSIONS

Co_{1-x}Ni_xFe₂O₄ (x=0.1-1.0) ferrites were synthesized using a hydrothermal method. The room temperature X-ray diffraction confirms the formation of single-phase Co-Zn ferrite at 180 °C. The average particle size determined with XRD data analysis is found to be in a range of 10.5-14.8 nm that decrease with Zn content. The photodegradation rate of methyl blue aqueous solutions on the nanoparticles decreases as increasing Zn content in the ferrites. The oxidation-reduction potential of methyl blue in aqueous solution in presence of the ferrite nanoparticles in sunlight is negative and increases as increase in Zn content, indicating decreased reductivity of the nanoparticles with increase in Zn content. The oxidation-reduction potential depends on the microstructure, light absorbance, and dark oxidation-reduction potential of the ferrite nanoparticles, and so synthetically reflected the photocatalytic activity of the nanoparticles.

ACKNOWLEDGEMENTS

The authors thank the Ms. Chen of the Shaanxi

ORIGINAL ARTICLE

university of science and technology for her kind assistance in SEM measurement.

REFERENCES

- [1] P.-G.Guo, G.-L.Zhang, J.-Q.Yu, H.-L.Li, X.-S.Zhao; Controlled synthesis, magnetic and photocatalytic properties of hollow spheres and colloidal nanocrystal clusters of manganese ferrite, *Colloids and Surf.A*, **395**, 168-174 (2012).
- [2] E.Casbeer, V.K.Sharma, X.-Z.Li; Synthesis and photocatalytic activity of ferrites under visible light: A review, *Sep.Purif.Technol.*, **87(5)**, 1-14 (2012).
- [3] A.Abd Aziz, K.S.Yong, S.Ibrahim, S.Pichiah; Enhanced magnetic separation and photocatalytic activity of nitrogen doped titania photocatalyst supported on strontium ferrite, *J.Hazard.Mater.*, **199-200(15)**, 143-150 (2012).
- [4] Y.-S.Fu, H.-Q.Chen, X.-Q.Sun, X.Wang; Combination of cobalt ferrite and graphene: High-performance and recyclable visible-light photocatalysis, *Appl.Catal.B: Environ.*, **111-112(12)**, 280-287 (2012).
- [5] T.E.Agustina, H.M.Ang, V.K.Vareek; A review of synergistic effect of photocatalysis and ozonation on wastewater treatment, *J.Photochem.Photobiol. C: Photochem.Rev.*, **6**, 264-273 (2005).
- [6] D.W.Bahnemann, J.Cunningham, M.A.Fox, E.Pelizzetti, P.Pichat, N.Serpone; in: R.G.Zepp, G.R.Heltz, D.G.Crosby, (Eds); *Aquatic surface photochemistry*, Lewis Publishers, Boca Raton, 261 (1994).
- [7] J.R.White, A.J.Bard; Electrochemical investigation of photocatalysis at cadmium sulfide suspensions in the presence of methylviologen, *J.Phys.Chem.*, **89**, 1947-1954 (1985).
- [8] S.Kaur, V.Singh; TiO_2 mediated photocatalytic degradation studies of Reactive Red 198 by UV irradiation, *J.Hazard.Mat.*, **141**, 230-236 (2007).
- [9] J.H.Jung, H.Kobayashi, K.J.C.van Bommel, S.Shinkai, T.Shimizu; Creation of novel helical ribbon and double-layered nanotube TiO_2 structures using an organogel template, *Chem.Mater.*, **14**, 1445-1447 (2002).
- [10] F.E.Massoth, D.A.Scarpiello; Catalyst characterization studies on the Zn-Cr-Fe oxide system, *J.Catal.*, **21**, 294-302 (1971).
- [11] Shiyama Tetsuro, (Eds); *The metal oxide and its catalysis*, Kodansha Scientific press, Tokyo, (in Japanese), 179-201 (1978).
- [12] H.-Y.He, J.-F.Huang, L.-Y.Cao, J.-P.Wu, Q.Shen; Catalytic and photocatalytic activity of ZnCr_2O_4 particles synthesized using metallo-organic precursor, *Mater.Technol.*, **23**, 110-113 (2008).
- [13] S.Singhal, J.Singh, S.K.Barthwal, K.Chandra; Preparation and characterization of nanosize nickel-substituted cobalt ferrites ($\text{Co}_{1-x}\text{Ni}_x\text{Fe}_2\text{O}_4$), *J.Solid State Chem.*, **178**, 3183-3189 (2005).
- [14] V.L.Mathe, A.D.Sheikh; Magnetostrictive properties of nanocrystalline Co-Ni ferrites, *Physica B*, **405**, 3594-3598 (2010).
- [15] R.Arulmurugan, G.Vaidyanathan, S.Sendhilnathan, B.Jeyadevan; Thermo-magnetic properties of $\text{Co}_{1-x}\text{Zn}_x\text{Fe}_2\text{O}_4$ ($x=0.1-0.5$) nanoparticles, *J.Magn. Magn.Mater.*, **303**, 131-137 (2006).
- [16] A.Tawfik, I.M.Hamada, O.M.Hemeda; Effect of laser irradiation on the structure and electromechanical properties of Co-Zn ferrite, *J.Magn.Magn. Mater.*, **250**, 77-82 (2002).
- [17] G.V.Duong, N.Hanh, D.V.Linh, R.Groessinger, P.Weinberger, E.Schafler, M.Zehetbauer; Monodispersed nanocrystalline $\text{Co}_{1-x}\text{Zn}_x\text{Fe}_2\text{O}_4$ particles by forced hydrolysis: Synthesis and characterization, *J.Magn.Magn.Mater.*, **311**, 46-50 (2007).
- [18] C.-K.Kim, J.-H.Lee, S.Katoh, R.Murakami, M.Yoshimura; Synthesis of Co-, Co-Zn and Ni-Zn ferrite powders by the microwave-hydrothermal method, *Mater.Res.Bull.*, **36**, 2241-2250 (2001).
- [19] F.Gözüak, Y.Köseoğlu, A.Baykal, H.Kavas; Synthesis and characterization of $\text{Co}_x\text{Zn}_{1-x}\text{Fe}_2\text{O}_4$ magnetic nanoparticles via a PEG-assisted route, *J.Magn.Magn.Mater.*, **321**, 2170-2177 (2009).
- [20] S.Yañez-Vilar, M.Sánchez-Andújar, C.Gómez-Aguirre, J.Mira, M.A.Señaris-Rodríguez, S.Castro-García; A simple solvothermal synthesis of MFe_2O_4 ($\text{M}^{1/4}\text{Mn}$, Co and Ni) nanoparticles, *J.Solid State Chem.*, **182**, 2685-2690 (2009).
- [21] C.-H.Lu, S.-J.Liou; Hydrothermal preparation of nanometer lithium nickel vanadium oxide powder at low temperature, *Mater.Sci.Eng.B*, **75**, 38-42 (2000).
- [22] P.Priyadharsini, A.Pradeep, P.Sambasiva Rao, G.Chandrasekaran; Structural, spectroscopic and magnetic study of nanocrystalline Ni-Zn ferrites, *Mater.Chem.Phys.*, **116**, 207-213 (2009).
- [23] X.-C.Shen, X.-Z.Fang, Y.-H.Zhou, H.Liang; Synthesis and characterization of 3-aminopropyltriethoxysilane-modified superparamagnetic magnetite nanoparticles, *Chem.Lett.*, **33**, 1468-1469 (2004).

- [24] M.Ma, Y.Zhang, W.Yu, H.-Y.Shen, H.-Q.Zhang, N.Gu; Preparation and characterization of magnetite nanoparticles coated by amino silane, *Colloids Surf.A*, **212**, 219-226 (2003).
- [25] H.Sozeri, Z.Durmus, A.Baykal; Structural and magnetic properties of triethylene glycol stabilized $Zn_xCo_{1-x}Fe_2O_4$ nanoparticles, *Mater.Res.Bull.*, **47**, 2442-2448 (2012).
- [26] S.-H.Xiao, W.-F.Jiang, L.-Y.Li, X.-J.Li; Low-temperature auto-combustion synthesis and magnetic properties of cobalt ferrite nanopowder, *Mater.Chem.Phys.*, **106**, 82-87 (2007).
- [27] H.-Y.He, P.Chen, L.-Y.Cao, J.Lu; Surface alkaline-acidic and photocatalytic properties of $MMoO_4$ ($M=Fe^{2+}, Co^{2+}, Ni^{2+}$) nanoparticles in different media conditions, *Res.Chem.Intermed.*, (in press).
- [28] H.-Y.He, L.-Y.Cao, Z.He, J.Lu; Surface characterisations and photocatalytic property of MWO_4 ($M=Fe^{2+}, Co^{2+}, Ni^{2+}$) nanoparticles, *Int.J.Nano and Biomaterials*, (in press).